High-overtone Bulk Acoustic Resonator as passive Ground Penetrating RADAR cooperative targets

J.-M Friedt,[1] A. Saintenoy,[2] S. Chrétien,[3] T. Baron,[4] É. Lebrasseur,[4] T. Laroche,[4] S. Ballandras,[4, a)] and M. Griselin[5]

[1)] *SENSeOR SAS, Besançon, France*[b)]

[2)] *IDES, UMR CNRS 8148, Université Paris Sud, France*

[3)] *Laboratoire de mathématiques, UMR CNRS 6623, Université de Franche Comté, Besançon, France*

[4)] *FEMTO-ST Time & Frequency, UMR CNRS 6174, Université de Franche-Comté, Besançon, France*

[5)] *ThéMA, UMR CNRS 6049, Université de Franche-Comté, Besançon, France*

(Dated: 11 March 2013)

RAdio-frequency Detection And Ranging instruments – RADARs – are widely used for applications aimed at measuring passive target velocity or ranging for various metrology applications such as ground position and localization. Within the context of using piezoelectric acoustic passive sensors as cooperative targets to RADARs probed through a radiofrequency (RF) link, this paper reports on investigating the compatibility of narrowband resonator architectures with the classical operation mode of wideband RADAR instruments. Since single mode resonators are hardly compatible due to the limited bandwidth of their spectrum, the investigation has been extended to High-overtone Bulk Acoustic Resonator (HBAR) whose comb of modes appears appropriate to the use with RADAR instruments. This analysis leads to consider HBARs as delay lines providing a comb of echos in the time domain rather than through the usual frequency comb considerations. Experimental measurements of HBAR responses are demonstrated using Ground Penetrating RADAR (GPR) instruments fitted with a variety of antennas, and thus operating in various frequency ranges, as well as the identification of the device temperature through the echo time delay computed as the cross correlation maximum position. Finally, the use of such cooperative targets for single reflector identification within a clutter of reflectors is theoretically considered with the proposal of a FDTD-based simulation method encompassing both passive dielectric reflectors and the contribution of buried passive acoustic sensors.

PACS numbers: 84.40.Xb,85.50.-n, 43.38.Rh

Keywords: wireless, battery-less, surface acoustic wave, resonator, high overtone, bulk acoustic resonator, RADAR, signal processing

[a)]S. Ballandras is also with SENSeOR SAS

[b)]Electronic mail: jmfriedt@femto-st.fr; `http://jmfriedt.free.fr`

I. INTRODUCTION

RAdio-frequency Detection And Ranging instruments – RADARs – are widely used for applications aimed at measuring passive target velocity (through Doppler shift of the incoming wave) or ranging (swept frequency source or pulse mode RADAR). The use of cooperative targets for providing additional information on the illuminated reflector was considered as part of Identification as Friend or Foe (IFF[1,2]), although cryptographic requirements are now only met by active systems triggered by an incoming interrogation signal, as also used in the marine RADAR beacons (also known as racon[3]). Most significantly, when using the RADAR for providing information about buried interfaces, passive targets are most appropriate since hardly accessible after being buried for future maintenance or power source replacement[4].

RADARs aimed at positioning a target – and specifically Ground Penetrating RADAR (GPR) – are intrinsically wideband radiofrequency (RF) sources. The emitted signal bandwidth B – either inverse of the pulse duration in a pulse-mode RADAR or the frequency span of a frequency modulated continuous wave (FM-CW) implementation – defines the target position resolution of the system. As an example for FM-CW, the unit cell[5] is $c/(2B)$ (with c the velocity of an electromagnetic wave in the medium), and thus a 1.5-meter resolution requires a bandwidth of 100 MHz, whatever the central operating frequency is.

RF acoustic transducers based on the propagation of a mechanical wave atop or within a piezoelectric substrate have been used as acousto-electrical components either as frequency selective devices (filter and resonator) or for analog signal processing (convolvers, correlators)[6]. More recently, their use as sensors has been emphasized by using on purpose crystalline orientations exhibiting significant drift with the physical quantity under investigation, including temperature[7–9], stress[10] and chemical compound detection[11,12]. Under such conditions, the wired link between the probing electronics and the sensor is readily replaced by a wireless link, bridging the gap with the hardware associated with RADAR measurement strategies[13]. However, all current developements require dedicated hardware for recovering the signal returned by the acoustic transducer[14–16].

The purpose of the presented work is to assess the use of acoustic transducers as passive cooperative targets for RADAR[17], and more specifically to propose an alternative to the classical delay line[18] allowing for higher compactness and/or resolution. As will be discussed in the first section of this paper, acoustic resonators are hardly compatible with wideband

interrogation strategies. As such devices exhibit a narrowband spectral signature by essence, the fraction of the energy of a short incoming RF pulse overlapping their transfer function is so small that low-losses in the resonator are compensated for by the minute fraction of energy transferred to the resonator. In terms of time domain, the incoming pulse duration is too short with respect to the resonator time constant defined as $Q/(\pi f)$, with Q the quality factor of the resonator operating at frequency f, to significantly load energy within the resonator. Furthermore, the signal returned from a resonator is only recorded for a few microseconds at most by commercially available hardware, since such durations are usually consistent with the hundreds of meters at most of the furthest dielectric interface detectable by GPR (in ice, a wave propagating at 170 m/μs is recorded for 20 μs if the interface is located at 1100 m, amongst the deepest interfaces detectable on the antarctic ice-shelf[19–22]). Thus, acoustic delay lines have appeared as most suitable as passive cooperative targets to GPR since they too are intrinsically wideband (or characterized in the time domain by narrow – a few sine waves – pulses) and hence well suited to GPR interrogation.

However, since delay lines only operate around a single (central) frequency, with typical bandwidths of 5 to 10 %, a given sensor can only be probed by a GPR operating in a given frequency band since the dipole antenna used with GPR exhibits a quality factor of about 3 (as observed on a Malå RAMAC 200 MHz antenna set located on concrete)[23].

Furthermore, with impulse GPR systems, the frequency spectrum of the propagating pulse is not well constrained as it depends on the surrounding medium electromagnetic properties. It might yield poor efficiency if the bandpass of the incident pulse no longer matches the delay line operating frequency. Thus, in the second section of this paper, a novel sensor configuration is considered based on High-overtone Bulk Acoustic Resonator (HBAR) used as passive cooperative targets for GPR interrogation. Earlier developments on HBAR[24–26] have focused on its resonance characteristics, with quality factor magnifying acoustic resonance in general, and high coupling yet robust design (as opposed to membrane-based resonators such as FBAR). Two characteristics are particularly inspected here, namely the multiple reflections to the incoming pulse and the wide operating frequency range yielding compatibility of a single sensor with multiple GPR configurations.

We thus demonstrate

- the use of an HBAR as a cooperative target to GPR measurement

- time-domain analysis of HBAR response as an alternative to the classical frequency measurement approach when probing the cooperative target with a wideband incoming signal,
- the use of a HBAR as a coupled resonator with the acoustic device used as a radiofrequency transponder to a passive (here switch) sensor
- the target localization and associated object identification

II. RESONATOR SUITABILITY TO GPR PROBING

Since delay lines are efficiently characterized in a wide frequency range and their time-domain response is extracted from the inverse Fourier transform of their spectral response, they act as natural cooperative targets to pulse-mode GPR. However, the use of a resonator as a cooperative target for a GPR must be investigated to determine the actual interest of the approach.

The efficiency of a resonator in such conditions requires two assessments when compared to delay lines:

- is the interrogation range equal or larger than that of a delay line ?
- is the physical quantity measurement more accurate when monitoring the resonance frequency than the time delay ?

It has already been demonstrated[27] that the transient time domain record of an unloading bulk acoustic wave (BAW) resonator can be used for the accurate measurement of its resonance frequency and quality factor. Those two characteristics are well suited to the characterization of the mass loading and viscoelastic interaction of an acoustic wave with its environment[28]. A 5 MHz resonator exhibiting a quality factor of about 5600 unloads with a time constant of 36 ms. In[28], the signal is recorded for a duration of 3.5 ms, so that the spacing between Fourier coefficients is 286 Hz. Reaching the 0.1 Hz resolution when identifying the oscillation frequency of the resonator requires an improvement of 2900 with respect to the expected frequency spacing from a Fourier transform: in the case of strongly decaying signals, such a result is achieved through non-linear fitting of the exponential decay factor (dissipation) and damped sine wave frequency identification.

However, the Fourier transform is the least accurate method for identifying the returned signal frequency, due to the lack of knowledge on the returned signal shape. Considering that a single (or dual in case of a differential measurement) frequency is returned, a strong assumption of sparsity (a single isolated sine wave characterizes the signal behaviour) can be added when processing the recorded signal. Advanced signal processing techniques[29,30] can then be implemented to improve frequency determination and therefore measurement accuracy, such as those used for instance in the field of Nuclear Magnetic Resonance (NMR)[31,32]. Applying such strategies to resonators acting as GPR cooperative target is thus worth considering.

A. Returned power

For a given free-space propagation loss, emitted power, receiver noise level and antenna gain, the power returned from the sensor is solely associated with its transfer function with respect to the incoming signal and transducer insertion loss. Using Parseval's theorem, we consider the incoming energy transfer to the transducer in the frequency domain. A GPR pulse is characterized by its large bandwidth, typically several tens of MHz around 100 MHz. Such a spectral width is appropriate when interrogating delay lines, but might be considered as a hindrance when probing narrowband resonators. The fraction of the incoming pulse energy transmitted to the resonator is equal to bandwidth ratio: a resonator with a quality factor of 12500 at 100 MHz exhibits a spectral bandwidth of 8000 Hz. A 25 MHz wide pulse hence only transfers about 3×10^{-4} of its energy to the resonator, or -35 dB (Fig. 1). Adding the intrinsic loss of a resonator better than -5 dB, the global resonator losses interrogated using a GPR pulse are of the same order of magnitude of typical delay line insertion losses (-30 to -45 dB[33,34]).

[FIG. 1 about here.]

Hence, while a delay line might use most of the bandwidth provided by the incoming GPR pulse, the intrinsic insertion loss of about -35 dB greatly reduces the efficiency of the transducer to generate a usable return signal. Nevertheless, piezoelectric materials being linear, some signal will always be returned, possibly at a power level below the detector noise level.

This yields to the conclusion that resonators and delay lines should provide comparable signal levels, with a returned signal -30 to -45 dB lower than the incoming pulse level. However, recovering a signal is only the first step towards a physical quantity identification. This conclusion is experimentally demonstrated using a 100 MHz fundamental mode AT-cut quartz resonator (ref. RS196, provided by Xeco, Cedar City, UT, USA) on the one hand, and a 100 MHz delay line manufactures in Y+128^o lithium niobate on the other hand[18] located on a concrete slab between the emitting and receiving antennas of a 100 MHz Malå unit controlled by a CU unit. Fig. 2 shows the response signals corresponding to these devices recorded by the GPR unit. One can observe that both devices return the same amount of energy. However, the time delay between successive pulses (SAW delay line response) is related to the physical quantity under investigation (e.g. through the phase of the Fourier transform of the returned signal), whereas interpreting the resonator returned information requires an accurate identification of the resonance frequency. The challenge thus lies in extracting an accurate frequency information from such a short record, as discussed below.

[FIG. 2 about here.]

B. Resonance frequency estimate

In ice sounding, a typical GPR unit records up to t =5 μs of the returned signal, sampled over a few thousand points. Therefore, a simple Fourier transform only provides a very rough estimate of the returned signal frequency (the Fourier transform provides a resolution of 1/t$\simeq$200 kHz), unusable for identifying the physical quantity under investigation. Assuming an absolute temperature drift of 80 ppm/K as currently observed on lithium niobate SAW cuts, a 1 K resolution requires, at 100 MHz, 25-fold resolution improvement through signal processing. So called superresolution techniques based on parametric models[35–38] have been tested on experimental datasets but have not led to sufficient resolution improvement to yield usable results.

1. Sparse frequency distribution and compressed sensing approach

The frequency identification approach, assuming a sparse frequency distribution[39,40], which was developed for this project (Fig. 3) is the following. We assume that the sig-

nal is a sum of sine waves corrupted by some Gaussian noise, *i.e.*, can be written as

$$s_t = \sum_{k \in \mathcal{K}} c_k \ \exp(2i\pi f_k t) + \epsilon_t, \ \text{t=1,...,T} \tag{1}$$

where $\mathcal{K}$ is the index set of frequencies, assumed to be symmetric, *i.e.*, if $k \in \mathcal{K}$, then $-k \in \mathcal{K}$. We also assume the symmetry of the frequencies, *i.e.*, $f_{-k} = -f_k$ in order for the signal to be real valued, and ϵ_t, $t = 1, \ldots, T$ is an i.i.d. Gaussian $\mathcal{N}(0\sigma_\epsilon^2)$ sequence. In practice, the set $\mathcal{K}$ is a large set, e.g., 2^{16}, whose size is tuned as a function of the desired precision. The problem of estimating the frequencies is then reduced to the problem of estimating the associated coefficients c_k, $k \in \mathcal{K}$ under sparsity constraint, *i.e.*, most c_k's are equal to zero. If the estimation criterion is a standard least-squares cost function, then the resulting minimization problem under sparsity constraint is NP hard to solve if the number of nonzero components is, *e.g.*, a linear function of the sample size. In our problem, we know *a priori* that only a few frequencies are meaningful. Thus, the estimation task could be reduced to enumerating all possible small symmetric subsets of $\mathcal{K}$ and perform a least square estimation of the corresponding coefficients. However, this may still be computationally hard. Notice moreover that looking for only one frequency may be computationally easier but hazardous in practice, in the case where more than one are present in the signal due to external physical reasons, leading to statistical bias. The approach adopted here is based on the recent discoveries underlying the field of Compressed Sensing. The idea is to incorporate a nonsmooth penalization term such as the ℓ_1-norm of the vector of coefficients $c = (c_k)_{k \in \mathcal{K}}$. The resulting least-squares estimation problem thus reduces to solving

$$\min_{c \in \mathbb{R}^{|\mathcal{K}|}} \ \frac{1}{2} \|s - \Phi c\|_2^2 + \tau \|c\|_1, \tag{2}$$

where Φ is the Fourier matrix given by $\Phi_{t,k} = \exp(2i\pi f_k t)$, $t = 1, \ldots, T$, $k \in \mathcal{K}$, and τ is a relaxation parameter depending on the standard deviation σ_ϵ. The estimator given by the solution of (Eq. 2) is often called the LASSO estimator. The minimization problem itself is also called "Basis Pursuit" in the signal processing litterature. Compressed Sensing is a very recent field of research initiated by E. Candès, J. Romberg and T. Tao[41] and D. Donoho[42]. Since then, an enormous amount of contributions have appeared ranging from purely mathematical investigations to very practical applications, in particular in medical imaging, analog-to-digital conversion, gene expression analysis, astronomy to name just a few. One alternative approach is the SPICE[43] algorithm: both methods take into account

the sparsity of the spectrum and can be expected to achieve similar performances as a function of the sparsity, since the SPICE method has recently been proven equivalent to a robust LASSO procedure[44]. Therefore, our proposal consisting of simultaneously estimating the noise variance and the frequencies could be implemented within the SPICE framework as well.

It was proved in[45] that the Compressed Sensing framework could be useful for frequency estimation. In[45] a theoretical justification is proposed for the tuning of the relaxation parameter τ, depending on the knowledge of σ_ϵ. More precisely, they prescribe

$$\tau = 2 \times (1 + 1/\log(T)) \times \sqrt{T \times \log(T) + T \times \log(4 \times \pi \times \log(T))} \times \sigma_\epsilon \tag{3}$$

In the present study, we incorporated a simple recursive technique discussed and analyzed in the recent work[29] designed to adapt to unknown variance. This technique procedes as follows: give an initial guess of the variance. Then, run the LASSO estimator (2), obtain a first estimate $\hat{c}^{(1)}$ of c and compute the residual $\hat{e}^{(1)} = s - \Phi\hat{c}^{(1)}$. Then, compute the empirical variance of $\hat{e}^{(1)}$ and inject the obtained value in formula (3) for τ. Repeat the procedure until convergence: in pratice 4 or 5 iterations usually suffice (Fig. 3). The resulting standard deviation on the frequency estimate, after removing the long term drift due to temperature shift, is sub-10 kHz.

[FIG. 3 about here.]

2. Spectral overlap

Furthermore, a significant drawback of resonators is that being narrowband, some conditions have been observed in which the resonance frequency happens to occur at a notch of the emitted GPR signal. Indeed, pulse-mode GPR does not generate a signal based on a forced frequency source, but emits a pulse whose transfer function is defined by the minimum insertion loss of the emitting antenna, which is itself dependent on the surrounding medium permittivity. Under some conditions (GPR located on a carpet over a thin concrete slab), the antenna tuned for a nominal frequency of 100 MHz exhibits a narrow notch in the emitted signal spectrum, and hence couples little energy in the resonator. This situation never occurs in wideband delay lines which always recover some energy from other parts of the interrogation signal spectrum, independently of narrow notches.

Thus, although resonators appear suitable for identification by tagging a cooperative target, extracting a useful physical quantity information from the returned signal frequency seems challenging using off-the-shelf pulse-mode GPR units. FM-CW GPR with high frequency resolution might be more suitable to such applications, but these instruments are less widespread than the impulse GPR considered here: the availability of flexible, programmable frequency sources (Direct Digital Synthesizers – DDS) with large bandwidths yet high stability (quartz controlled) might provide new instrumentation opportunities in this direction.

III. HBAR SUITABILITY TO GPR PROBING

HBAR is a bulk acoustic resonator configuration in which the transduction single crystal layer is separate from the low-acoustic loss substrate. Separating these two materials allows for selecting the best conditions for each purpose: high coupling for the active (thin) film layer, and controlled temperature coefficient and low acoustic losses in the energy storage (thick) layer. Increased operating frequencies are reached by using a thin active layer, typically less than 50 μm thick, while mechanical strength is obtained by keeping the low loss substrate at 350 or 500 μm thicknesses. In our case, the stack of materials is obtained by room-temperature high-pressure bonding of two wafers and the thin piezoelectric film is obtained by lapping and polishing one of the stack materials. The buried metallic electrode – two gold films acting as adhesive layer as well – is kept at floating potential and two aluminum electrodes patterned on the HBAR surface are used for acoustic mode excitation through the inverse piezoelectric effect[46–48].

A. HBAR as time domain delay lines

[FIG. 4 about here.]

One of the HBAR characteristics – multiple equidistant reflections in the time domain – is best apprehended by considering that the Fourier transform of a comb is a comb (Fig. 4). The classical design approach for HBAR is to consider that overtones are confined in a thick substrate: the frequency-domain of the transducer is a comb whose mode spacing is defined by the ratio between the equivalent phase velocity of the mode propagating in the material

stack and its thickness (a thick substrate geometric properties), while the mode coupling is modulated on a wider frequency range by the thin excitation film geometric properties. Typical comb spacing for a $t = 350$ μm-thick low-loss substrate is $t/v = 11$ MHz with v the acoustic wave velocity assumed to be around 4000 m/s. The tranducer film thickness is usually tuned to be a few micrometers thick so that the envelope maximizes modes in the range under consideration, as well as its odd overtones. Thus, a 40 μm thick film would exhibit a transfer function maximizing mode coupling at 100, 300, 500 MHz, etc. Hence, such a device is compatible with multiple GPR antenna configurations and most substrates since some modes will always be excited by the incoming electromagnetic pulse.

[FIG. 5 about here.]

The time-domain characterization of an HBAR is a direct consequence of the small spacing between modes. The impulse response of a comb in the frequency domain of modes separated by 11 MHz is a series of pulses separated by 91 ns (dependent on the acoustic velocity and the substrate thickness as explained in the previous section). Thus, the interest will be focused here on the propagation delay between adjacent echos.

As opposed to microwave RADAR receivers which require a preliminary demodulation stage to bring the signal within the sampling range[15], GPR operates at low enough frequency for the baseband signal to be sampled. Thus, rather than exploiting the phase difference of adjacent pulses as done on classical acoustic delay line wireless interrogation units[49], a matched filter approach provides on the one hand an optimum differential measurement strategy for improving the chances of detecting the returned signal in the noisy receiver signal – since all reflected echos are affected by the same correlated channel noise – and to identifiy accurately the time delay between adjacent pulses, thus yielding the acoustic velocity which is related to the physical quantity under investigation.

Differential measurement based on the time delay between returned echos, rather than an absolute delay measurement, is mandatory to extract the physical quantity independently of the RADAR to sensor distance, and to reduce the influence of the local oscillator drift[50–53] when computing a time delay.

The cross correlation is used as a natural optimum filter for identifying the distance between adjacent reflections. With this process, even short (a few microsecond long) reflected signal records (as provided by a GPR receiver) provide the means to recover accurate tem-

perature informations when using an HBAR as temperature probe (Figs 4 and 5, top). While a cross correlation approach would yield to the asymptotic capability of detecting a vanishingly small periodic signal in noise, the analysis of finite duration samples has been considered in[54]: the cross-correlation of the multiple noisy representations of the echos returned by the sensor are demonstrated to perform worse than the ideal case of correlating with a noise-free representation of the emitted pulse, but the latter approach does not allow for accounting for varying emission pulse characteristics (as found with varying soil environments in GPR) or sensor impedance variation.

B. Interrogation range assessment

While the coupling of single mode resonators reveals inefficient due to the broadband incoming pulse, the excitation of multiple adjacent modes as occurring in HBARs provides the framework for using at best the cross correlation and thus for efficiently extracting the transducer signature from noisy signals. Indeed, adjacent modes exhibit similar wave shapes, and thus the cross-correlation of adjacent time-domain echos exhibits a maximum for an offset defining the time delay between the echos. Polynomial fit around the cross-correlation maximum allows for a significant resolution improvement related to the signal to noise ratio, typically reaching 100.

Cross correlation analysis of successive pulses exhibits two advantages: i) the cross correlation provides matched filtering and thus improved signal extraction from noise with no preliminary knowledge on the emitted pulse shape, and ii) the cross correlation maximum provides an accurate estimate of the time delay between adjacent pulses. Taking advantage of the signal extraction capability of the matched filter approach, an interrogation range of 5 m has been experimentally observed in snow (Fig. 5, bottom).

C. Temperature measurement using 100, 200 and 250 MHz GPR units

As an experimental demonstration of these concepts, a HBAR made of a stack of two lithium-niobate single-crystal wafers was probed using Malå CU and CU2 GPR units. These control units were fitted with 100, 200 MHz unshielded antennas and a set of 250 MHz shielded antennas. Since an avalanche transistor unloads in a dipole antenna with a time

constant defined by the transfer function of the antenna, changing the dipole length is enough to change the operating frequency of the RADAR emitter. A wideband receiver records any returned echo reflected from buried dielectric and conductivity interfaces or, in our case, echos returned by the acoustic transducer acting as a passive sensor. All signal processing for recovering the acoustic velocity and thus the physical quantity to measure are performed as digital post-processing on the recorded data: no hardware modification on the GPR unit is needed for recording the data.

The HBAR temperature dependence was first calibrated, and during the experimental assessment of the interrogation of the acoustic transducer with a GPR, the sensor was fitted with a 1-ohm resistor acting as a heater and a Pt100-probe for independent temperature measurements (Fig. 6).

[FIG. 6 about here.]

The design of HBAR dedicated to temperature sensing involves the integration of multiple design challenges:

- the thin piezoelectric film thickness must be tuned so that the envelope of the transfer function exhibits maxima around the operating frequency ranges of the available GPR antenna, in our case 100, 200 and 250 MHz for example,

- the thick substrate thickness must be tuned in such a way that the multiple echos are detected by the RADAR within the sampling duration, while being spaced enough to allow for individual pulse identification in order to perform the cross-correlation time delay measurement,

- the selection of substrate material maximizes the coupling in order to extend the interrogation range, while the temperature sensitivity dependence with the overtone number is defined by the energy distribution between the transducer film material and the thick (resonating) substrate.

- electrode dimensions in order to match the impedance of the antenna when buried in soil, considering the permittivity and thickness of the thin piezoelectric film (static capacitance) and its electromechanical coupling (impedance at resonance).

The complexity of such a sensor design is illustrated in Fig. 7 in which the first order thermal sensitivity of an HBAR made of a stack of lithium niobate on quartz is modelled. The lithium niobate orientation selected in this case generates shear waves. Considering a constant substrate thickness, the thinner the piezoelectric layer, the lower the dependence of the first order temperature coefficient of frequency (TCF) versus the overtone number is. Different lithium niobate cuts – *e.g.* for generating longitudinal wave, will exhibit different TCF dependence with overtone number. However, the piezoelectric layer thickness is defined by the operating frequency condition, so that tuning this design parameter is not an option for addressing the temperature sensitivity dependence with the overtone number. The remaining option is the selection of a different substrate material minimizing the dependence of the sensitivity with the overtone number, or a preliminary detailed modelling of the dependence of all overtone frequencies with the physical quantities under consideration. Nevertheless, these considerations are discussed to emphasize that GPR measurements of a same sensor probed at various frequencies (using various antenna sets) might not be trivially compared and might yield different results if the sensitivity dependence of the various overtones probed is not considered.

[FIG. 7 about here.]

D. HBAR as 4-pole coupled transducers

So far, the intrinsic HBAR properties associated with the material velocity change have been considered as a function of environmental physical properties. However, in a coupled oscillator approach, the transfer function of the HBAR might be affected by impedance changes of an external load (Fig. 8)[55–57]. Indeed, the electrode configuration we consider (Fig. 6, top right) avoids etching the piezoelectric layer to reach the buried electrode and rather keeps the buried electrode at floating potential. In the 2-port configuration considered so far (Port1 and ground as shown on Fig. 6), one electrode is connected to the antenna while the surrounding electrode is at ground. In a 4-port configuration (Port1 and Port2 with respect to the common ground on Fig. 6), a second electrode is used and the evanescent wave from one electrode couples with the acoustic field from the second electrode. Typical sensor size is 1×1 mm^2 and electrode diameter is 900 μm.

While it is classically known that a load will affect the reflection coefficient and delay of an acoustic delay line when connected to one of the reflecting mirrors (either tuning a capacitance due to moisture level changes[58] or tuning a resistance through magnetic field variations[59]), the coupled resonator approach uses some energy sharing between two resonating structures, with one used as the RF transducer and the other as the second-set of ports (4-port device) to which the load is connected. In our demonstration, a 50 Ω is either connected (closed switch) or disconnected (open port, representing an open switch) to the second port, while the first port is connected to a dipole antenna and acts as the RF transducer (Fig. 8).

[FIG. 8 about here.]

Various propagation modes (longitudinal and transverse polarization) have been operated, yielding various coupling efficiencies. Indeed, while the propagation of longitudinal waves yields high sensitivity of the RF transducer to the load impedance, shear waves exhibit on the opposite a very low sensitivity of the velocity to the load. This tuning capability, added to the geometrical degrees of freedom (electrode dimensions and electrode spacings), are the necessary parameters for designing a transducer best suited for different purposes: a transducer of an impedance load sensor, an intrinsic temperature sensor (if using high TCF substrates), or a intrinsic stress/pressure sensor (if using low TCF substrates aiming at temperature compensation over the operating range).

E. Sensor localization

Clutter[60] – the set of reflectors hiding the targeted objects – has been classically removed in airborne radar surveys through Doppler filtering[5] (removing static targets to only keep the moving targets assumed to be of interest) and is compatible with synthetic aperture antenna scanning[61]. Such a strategy is obviously not applicable to classical static buried targets.

When acquiring a mono-offset GPR profile along the surface, the signal of a small reflector embedded in a homogeneous medium of velocity c is characteristic. The two-way travel time $2t$ needed to reach the reflector at depth d as the antennas are scanned along the x axis is

the classical[62] hyperbola equation

$$4c^2t^2 = x^2 + d^2 \Leftrightarrow \frac{4c^2}{d^2}t^2 - \frac{1}{d^2}x^2 = 1$$

whose curvature is

$$\frac{\partial^2 t}{\partial x^2} = \frac{d^2}{2c\left(d^2 + x^2\right)^{3/2}}$$

which is equal, above the reflector ($x = 0$) to $1/(2dc)$. Then, when an hyperbola is discernable in a radargram, its analysis gives all the parameters to locate the corresponding reflector. Some classical reflection data analysis called migration[63,64] allows for the convergence of all the energy scattered along the hyperbola at its apex. However the migration does not always allow for a precise identification of the target as it will be illustrated later in a numerical example.

In a heterogeneous medium presenting two many scaterrers, one way of identifying a given target among the clutter was considered consisting in delaying its returned echo by a time delay[62] longer than the distance at which the reflectors acting as clutter are located. Because the hyperbola curvature of the reflected echo time delay is dependent on both the point-like reflector depth and medium velocity as a function of antenna position, assuming a constant velocity through out the probed volume, the migration process will uniquely converge for the set of echos delayed by the acoustic transducer. All other reflectors which might remain at the equivalent depth of the returned echo delay will still be seen as hyperbolae after migration, with a lower energy density allowing for an automated threshold detection of the successful migration algorithm for the signals associated with the acoustic sensor.

Getting rid of clutter not only improves the chances of isolating the wanted target, but also optimizes the migration process by improving the signal to noise ratio, and thus the vertical localization accuracy (the spatial localization is always limited by the hyperbola curvature and the ability of the operator to identify the hypervola summit). In order to assess such a statement, 2D Finite-Difference Time-Domain (FDTD) simulations of the radargrams supposedly obtained by a 200 MHz scanning perfectly conducting reflectors buried in $\varepsilon_r = 3$ homogeneous dry sand were performed (GprMax2D software[65]), yielding a wavelength in the dielectric environment of 86 cm. The resulting datasets were then migrated using Stolt algorithm[63] (as implemented in Seismic Unix software package[66]). The optimum electromagnetic velocity was searched for by maximizing the energy at the reflector convergence of all the migrated hyperbolas (Fig. 9).

[FIG. 9 about here.]

The challenge in using available FDTD software is related to the linearity of the acoustic sensor response: the piezoelectric transducer electromechanical conversion will indeed generate a delayed echo from the main incoming RF impulse as well as any other secondary energy sources, but with an attenuation combining the intrinsic sensor losses as well as the low reflection coefficient of the passive interface. Furthermore, the acoustic sensor acts itself as a buried RF source whose emitted echos are themselves reflected by any buried interface. Thus, we propose a two-step simulation approach, in which a mobile emitting source raster-scans the measurement surface while the receiver is kept static at the sensor location and the time-dependent electromagnetic field values are recorded. In a second step, these values are delayed in time, possibly repeated multiple times to match the multiple echos of the HBAR acting as a delay line, and the source now remains static at the sensor location while the GPR receiver raster scans the surface. While GprMax2D allows for such functionalities, the remaining issue is the modelling of the buried source which is assumed to be defined by an electrical current. The derivation of the current distribution from the electromagnetic fields is as follows:

1. the buried receiver records the TE E_z electric field where the sensor is assumed to be located,

2. from the Maxwell-Faraday relation between current density $\vec{J}$ and electric field $\vec{E}$

$$\nabla \wedge (\nabla \wedge (\vec{E})) = -\mu_0 \frac{\partial \vec{J}}{\partial t}$$

   so that the current distribution is related to the time integral of the electric field,

3. in a 2D expression of the discretized FDTD, $\nabla \wedge (\nabla \wedge (\vec{E}))$ is expressed as

$$\frac{\partial^2 E_z}{\partial x^2} + \frac{\partial^2 E_z}{\partial y^2} = \mu_0 \frac{\partial J_z}{\partial t} = -2\frac{E_z}{\Delta x^2} - 2\frac{E_z}{\Delta y^2}$$

   under the assumption that the electric field values adjacent to the pixel considered in the discretized second order derivative are null, as required by the point-like source description,

4. having recorded the received time dependent E_z field, a convolution is performed with the acoustic transducer time-response, which in a first approximation is considered

as a comb of Dirac functions (although the convolution with the experimental S_{11} transfer function would match actual experimental conditions), and the time integral is computed to generate the new source $J_z(t)$,

5. a second FDTD simulation is performed with this new buried source and the receiver located on the surface. Thus, all reflections of the sensor returned echos on the buried interfaces will be displayed.

This approach is validated by the fact that adding the Maxwell-Ampère relation between magnetic and electric fields, the deduced current propagation law

$$\nabla \wedge (\nabla \wedge (\vec{J})) = -\mu_0 \varepsilon_0 \varepsilon_r \frac{\partial^2 \vec{J}}{\partial t^2}$$

indeed follows a propagating wave relation. We demonstrate this complete modelling process including the buried acoustic transducer acting as a delayed source in Fig. 10.

[FIG. 10 about here.]

While the linearity of the piezoelectric effect will induce a sensor response from all multiple reflections between buried interfaces, the noise level of the GPR RF receiver will act as a threshold on the received signal. Practically, while all multiple reflection paths should be considered[67], only the first few reflectors with significant RADAR cross sections will return a detectable amount of energy to the GPR receiver.

IV. CONCLUSION

We have first considered acoustic resonators as alternative to acoustic delay lines acting as cooperative targets for wideband RADARs. Due to their narrowband response, the poor spectrum matching with the transmitted radiofrequency pulses compensates for the intrinsic low losses of resonators, and the interrogation range is expected to be about the same than the one observed for delay line. However, accurate identification of the resonance frequency from such short time samples appears challenging and signal processing for extracting a physical quantity value is significantly more complex in the case of resonators than in the case of delay lines.

We have then demonstrated how High-overtone Bulk Acoustic Resonators (HBAR) do provide multiple advantages as cooperative targets probed by Ground Penetrating RADAR

(GPR) acting as sensors: wideband operating conditions with respect to single-mode delay lines, compatible with varying operating frequencies of RADAR units depending on soil permittivity, and time-domain response relevant for temperature measurement as opposed to the challenging resonance frequency identification of resonators. Furthermore, beyond the measurement of physical quantities affecting the equivalent velocity of acoustic waves in the HBAR material stack, delaying the reflected signal improves the target localization capability of GPR by delaying the useful signal far beyond clutter reflections.

Some of the sensor design challenges were addressed, including the varying temperature sensitivity of the various overtones of HBARs due to varying energy distribution in the different materials the transducer is made of. Depending on the targeted measurement accuracy, minimizing this variation might be needed, while on the other hand multi-parametric measurements using a single transducer might take advantage of widely varying sensitivities of the various overtones to different physical parameters.

ACKNOWLEDGEMENT

J.-P Simonnet (Chronoenvironnement, Univ. Franche-Comté, Besançon, France), provided access to one of the GPR units used in these experiments. Funding for the development of the sensors was partly provided by the Agence Nationale de la Recherche (ANR) CryoSensor program. The authors would also like to thank Ben Recht (Computer Sciences Department, Univ. of Wisconsin, USA) for generously sharing the latest version of the Matlab code described in[45]. The associated code[68] is available at `www.lx.it.pt/~mtf/SpaRSA` (last accessed Aug. 2012). We show gratitude to Dr. A. Giannopoulos (Univ. of Edinburgh UK), for generously sharing his closed-source GPRMax program available at `www.gprmax.org`.

REFERENCES

[1]M. Rieback, B. Crispo, and A.S. Tanenbaum. The evolution of RFID security. *IEEE Pervasive Computing Magazine*, 5(1):62–69, January-March 2006.

[2]K.L. Lerner and B.W. Lerner. *Encyclopedia of Espionnage, Intelligence and Security*, volume 2. Thomson Gale, Farmington Hills, MI, USA, 2004.

[3]A. Bole, B. Dineley, and A. Wall. *Radar and ARPA manual: radar and target tracking for professional mariners, yachtsmen and users of marine radar, 2nd Ed.* Elsevier Butterworth-Heinemann, Oxford, UK, 2005.

[4]C.T. Allen, K. Shi, and R.G. Plumb. The use of ground-penetrating radar with a cooperative target. *IEEE Transactions on Geoscience and Remote Sensing*, 5(2):1821–1825, 36 1998.

[5]M. Skolnik. *Radar handbook, 3rd Ed.* McGraw-Hill Professional, January 2008.

[6]C. Campbell. *Surface Acoustic Wave Devices and Their Signal Processing Applications.* Academic Press, April 1989.

[7]X Q. Bao, W. Burfhand an V.V. Varadan, and V.K. Varadan. SAW temperature sensor and remote reading system. In *IEEE Ultrasonics Symposium*, pages 583–585, Denver, CO, USA, 1987.

[8]W. Buff, S. Klett, M. Rusko, J. Ehrenpfordt, and M. Goroli. Passive remote sensing for temperature and pressure using SAW resonator devices. *IEEE Transactions on Ultrasonics, Ferroelectrics, and Frequency Control*, 45(5):1388–1392, September 1998.

[9]G. Bruckner, A. Stelzer, L. Maurer, J. Biniasch, L. Reindl, R. Teichmann, and R. Hauser. A high-temperature stable SAW identification tag for a pressure sensor and a low-cost interrogation unit. In *11th International Sensor Congress (SENSOR)*, pages 467–472, Nuremberg, Germany, 2003.

[10]A. Pohl, R. Steindl, and L. Reindl. The "intelligent tire" utilizing passive SAW sensors – mesurement of tire friction. *IEEE Transactions on Instrumentation and Measurement*, 48(6):1041–1046, december 1999.

[11]Y. Dong, W. Cheng, S. Wang, Y. Li, and G. Feng. A multi-resolution passive SAW chemical sensor. *Sensors and Actuators B*, 76:130–133, 2001.

[12]W. Wang, C. Lim, K. Lee, and S. Yang. Wireless surface acoustic wave chemical sensor for simultaneous measurement of co_2 and humidity. *J. Micro/Nanolith. MEMS MOEMS*, 8(3):031306, 2009.

[13]F. Schmidt, O. Sczesny, L. Reindl, and V. Mhgori. Remote sensing of physical parameters by means of passive surface acoustic wave devices ("ID-TAGS"). In *IEEE Ultrasonics Symposium*, pages 589–592, 1994.

[14]A.Pohl, F.Seifert, L.Reindl, G.Scholl, T. Ostertag, and W.Pietsch. Radio signals for SAW ID tags and sensors in strong electromagnetic interference. In *IEEE Ultrasonics Sympo-*

sium, pages 195–198, Cannes, France, 1994.

[15]M. Hamsch, R. Hoffmann, W. Buff, M. Binhack, and S. Klett. An interrogation unit for passive wireless SAW sensors based on Fourier transform. *IEEE Transactions on Ultrasonics, Ferroelectrics, and Frequency Control*, 51(11):1449–1456, november 2004.

[16]A. Stelzer, S. Schuster, and S. Scheiblhofer. Readout unit for wireless SAW sensors and ID-tags. In *International Workshop on SiP/SoC Integration of MEMS and Passive Components with RF-ICs*, 2004.

[17]A. Stelzer, G. Schimetta, L. Reindl, A. Springer, and R. Weigel. Wireless SAW sensors for surface and subsurface sensing applications. In *SPIE Proceedings – Subsurface ans Surface Sensing Technologies and Applications III*, volume 4491, pages 358–366, 2001.

[18]J.-M Friedt, T. Rétornaz, S. Alzuaga, T. Baron, G. Martin, T. Laroche, S. Ballandras, M. Griselin, and J.-P. Simonnet. Surface acoustic wave devices as passive buried sensors. *Journal of Applied Physics*, 109(3):034905, 2011.

[19]R.W. Jacobel, S.M Hodge, and D.L. Wright. Studies of internal layering and bedrock topography on ice stream C, West Antartica. *Antarctic Journal of the United States*, 25(5):82–85, 1990.

[20]D.-L Wright, S.M. Hodge, J.A. Bradley, T.P. Grover, and R.W. Jacobel. A digital low-frequency, surface-profiling ice-radar system. *Journal of Glaciology*, 36(122):112–121, 1990.

[21]L. Cafarella, S. Urbini, C. Bianchi, A. Zirizzotti, I.E. Tabacco, and A. Forieri. Five subglacial lakes and one of antartica's thickest ice covers newly determined by radio echo sounding over the vostok-dome c region. *Polar Research*, 25(1):69–73, 2006.

[22]A.P. Kapista, J.K. Ridley, G de Q. Robin, M.J. Siergert, and I.A. Zotikov. A large deep freshwater lake beneath the ice of central east antartica. *Nature*, 381:684–686, June 1996.

[23]T. Wunderlich and W. Rabbel. Absorption and frequency shift of GPR signals in sandy and silty soils: Empirical relations between Q, complex permittivity and the clay and water contents. *Near Surface Geophysics*, to be published, 2012.

[24]H. Zhang, W. Pang, H. Yu, and E.S. Kim. High-tone bulk acoustic resonators on sapphire, crystal quartz, fused silica, and silicon substrates. *J. Appl. Phys.*, 99(12):124911, 2006.

[25]G.D. Mansfeld. Theory of high overtone bulk acoustic wave resonator as a gas sensor. In *13th International Conference on Microwaves, Radar and Wireless Communications. 2000. MIKON-2000*, volume 2, pages 469–472, 2000.

[26]M.M. Driscoll, R.A. Jelen, and N. Matthews. Extremely low phase noise uhf oscillators utilizing high-overtone, bulk-acoustic resonators. *IEEE Trans. Ultrason. Ferroelectr. Freq. Control*, 39(6):774–9, 1992.

[27]M. Rodahl and B. Kasemo. A simple setup to simultaneously measure the resonant frequency and the absolute dissipation factor of a quartz crystal microbalance. *Rev. Sci. Instrum.*, 67(9), September 1996.

[28]M. Rodahl, F. Höök, A. Krozer, P. Brzezinski, and B. Kasemo. Quartz crystal microbalance setup for frequency and Q-factor measurements in gaseous and liquid environments. *Rev. Sci. Instrum.*, 66(7), July 1995.

[29]S. Chrétien and S. Darses. Sparse recovery with unknown variance: a LASSO-type approach, 2012. available at `http://arxiv.org/abs/1101.0434`.

[30]S.J. Wright, R.D. Nowak, and M.A.T Figueiredo. Sparse reconstruction by separable approximation. *IEEE Transactions on Signal Processing*, 57(7):2479–2493, July 2009.

[31]V.A. Mandelshtam and H.S. Taylor. Harmonic inversion of time signals. *J. Chem. Phys.*, 107(17):6756–6769, 1997.

[32]H. Hu, Q. N. Van, V. A. Mandelshtam, and A. J. Shaka. Reference deconvolution, phase correction, and line listing of NMR spectra by the 1D filter diagonalization method. *J. Magnetic Resonance*, 134:76–87, 1998.

[33]G. Scholl, C. Korden, E. Riha, C.C.W. Ruppel, U. Wolff, G. Riha, L. Reindl, and R. Weigel. SAW-based radio sensor systems for short-range applications. *IEEE Microwave magazine*, pages 68–76, December 2003.

[34]T.F. Bechteler and H. Yenigün. 2-D localization and identification based on SAW ID-tags at 2.5 GHz. *IEEE Trans. on microwave theory and techniques*, 51(5), 2003.

[35]R. Carriere and R.L. Moses. High resolution radar target modeling using a modified prony estimator. *IEEE Trans. Antennas Propogat.*, 40:13–18, January 1992.

[36]D. Tufts and R. Kumaresan. Singular value decomposition and improved frequency estimation using linear prediction. *IEEE Transactions on Acoustics, Speech and Signal Processing*, 30(4):671–675, 1982.

[37]Y. Kai-Bor M.D. Rahman. Total least squares approach for frequency estimation using linear prediction. *IEEE Transactions on Acoustics, Speech and Signal Processing*, 35(10):1440–1454, 1987.

[38]S. Chrétien and I. Dologlou. Successive projection-like algorithms for signal approximation/zero error modelling. In *Proc. IEEE international conference on acoustics, speech and signal processing*, pages 1240–1243, Detroit, USA, 1995.

[39]H. Li, P. Stoica, and J. Li. Computationally efficient parameter estimation for harmonic sinusoidal signals. *Signal Processing*, 80:1937–1944, 2000.

[40]K. W. Chan and H. C. So. Accurate frequency estimation for real harmonic sinusoids. *IEEE Signal Processing Letters*, 11(7):609–612, 2004.

[41]E. Candes, J. Romberg, and Tao T. Robust uncertainty principles: Exact signal reconstruction from highly incomplete frequency information. *IEEE Information Theory*, 2(52):489–509, 2006.

[42]D. Donoho. Compressed sensing. *IEEE Trans. on Information Theory*, 52(4):1289–1306, 2006.

[43]P. Stoica, P. Babu, and J. Li. SPICE: A Sparse Covariance-Based Estimation Method for Array Processing. *IEEE Transactions on Signal Processing*, 59:629–638, 2011.

[44]C.R. Rojas, D. Katselis, and H. Hjalmarsson. A note on the SPICE method. *arXiv:1209.4887*, 2012.

[45]B. Bhaskar, G. Tang, and B. Recht. Atomic norm denoising with applications to line spectral estimation. In *Proceedings of the 49th Annual Allerton Conference*, 2011. Extended version available at `http://arxiv.org/abs/1204.0562`.

[46]D. Gachon, É. Courjon, J. Masson, V. Pétrini, J. Y. Rauch, and S. Ballandras. *linbo*$_3$-*linbo*$_3$ high overtone bulk acoustic resonator exhibiting high $q.f$ product. In *IEEE Ultrasonics Symposium – IUS*, pages 1417–1420, 2007.

[47]T. Baron, É. Lebrasseur, J.-P. Romand, S. Alzuaga, S. Queste, G. Martin, D. Gachon, T. Laroche, S. Ballandras, and J. Masson. Temperature compensated radio-frequency harmonic bulk acoustic resonators pressure sensors. In *IEEE Ultrasonics Symposium – IUS*, pages 2040–2043, 2010.

[48]S. Ballandras, T. Baron, É. Lebrasseur, G. Martin, S. Alzuaga, J.-M. Friedt, J.C. Poncot, and C. Guichard. High overtone bulk acoustic resonators built on single crystal stacks for sensors applications. In *IEEE Sensors proceedings*, pages 516–519, 28-31 Oct. 2011.

[49]J.H. Kuypers, L.M. Reindl, S. Tanaka, and M. Esashi. Maximum accuracy evaluation scheme for wireless saw delay-line sensors. *IEEE Transactions on Ultrasonics, Ferroelectrics and Frequency Control*, 55(7):1640–1652, July 2008.

[50]T. E. Parker. Analysis of aging data on SAW oscillators. In *Proc. 34th Ann. Symp. on Frequency Control*, pages 292–301, 1980.

[51]W. R. Shreve, J.A. Kusters, and C.A. Adam. Fabrication of SAW resonators for improved long term aging. In *Proc. 1978 Ultrasonics Symp.*, pages 573–579, 1978.

[52]W. R. Shreve. Active aging of SAW resonators. In *Proc. 1980 Ultrasonics Symp.*, pages 188–192, 1980.

[53]J. R. Vig. Resonator aging. In *IEEE Ultrasonics Symposium Proceedings*, pages 848–849, 1977.

[54]Y.W. Lee, T.P. Cheatham, and J.B Wiesner. The application of correlation functions in the detection of small signals in noise. Technical Report Technical report 141, Massachussets Institute of Technology, 1949.

[55]Y.S. Huang, Y.Y. Chen, and T.T. Wu. A passive wireless hydrogen surface acoustic wave sensor based on Pt-coated ZnO nanorods. *Nanotechnology*, 21(9):095503, Mar 5 2010.

[56]J.-G. Oh, B. Choi, and S.-Y. Lee. SAW based passive sensor with passive signal conditional using MEMS A/D converter. *Sensors and Actuators A*, 141:631–639, 2008.

[57]J.-G. Kim, T.-J. Lee, N.-C. Park, Y.-P. Park, K.-S. Park, S.-C. Lim, and W.-S. Ohm. SAW-based capacitive sensor with hemispherical electrode for nano-precision gap measurement. *Sensors and Actuators A*, 163:54–60, 2010.

[58]L. Reindl, C.C.W. Ruppel, A. Kirmayr, N. Stockhausen, M.A. Hilhorst, and J. Balendonck. Radio-requestable passive SAW water-content sensor. *IEEE Trans. on Microwave theory and techniques*, 49(4):803–808, 2001.

[59]L.M. Reindl, A. Pohl, G. Scholl, and R. Weigel. SAW-based radio sensor systems. *IEEE Sensors journal*, 1(1):69–78, 2001.

[60]C. Rappaport, M. El-Shenawee, and H. Zhan. Suppressing GPR clutter from randomly rough ground surfaces to enhance nonmetallic mine detection. *Subsurface Sensing Technologies and Applications*, 4(4):311–326, October 2003.

[61]J.K. Jao. Theory of synthetic aperture radar imaging of a moving target. *IEEE Transactions on Geoscience and Remote Sensing*, 39(9), September 2001.

[62]C.T. Allen, K. Shi, and R.G. Plumb. Characterization of a cooperative target for ground-penetrating radar. In *Proceedings of the 7th International Conference on Ground Penetrating Radar (GPR '98)*, pages 561–565, Lawrence, Kansas, May 1998.

[63]R. H. Stolt. Migration by Fourier transform. *Geophysics*, 43(1):23–48, February 1978.

[64]T.D. Dorney, J.L. Johnson, J. Van Rudd, R.G. Baraniuk, W.W. Symes, and D.M. Mittleman. Terahertz reflection imaging using Kirchhoff migration. *Optics Letters*, 26(19):1513–1515, 2001.

[65]A. Giannopoulos. Modelling ground penetrating radar by GprMax. *Construction and Building Materials*, 19(10m):755–762, 2005.

[66]Jr. J.W. Stockwell. The CWP/SU: Seismic un*x package. *Computers and Geosciences*, May 1999.

[67]G. Stuart, T. Murray, N. Gamble, K. Hayes, and A. Hodson. Characterization of englacial channels by ground-penetrating radar: An example from austre Brøgerbreen, Svalbard. *Journal of Geophysical Research*, 108:2525, 2003.

[68]S.J. Wright, R. Nowak, and M.A. T. Figueiredo. Sparse reconstruction by separable approximation. *IEEE Transactions on Signal Processing*, 57:2479–2493, 2009.

LIST OF FIGURES

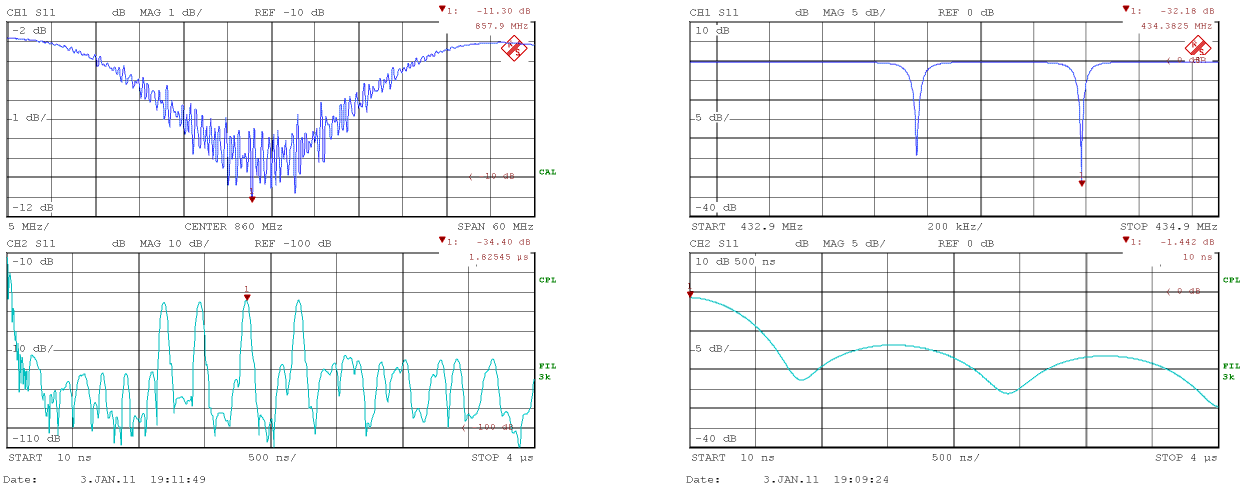

(a) (b)

FIG. 1. Frequency domain (top) and time domain (bottom) characterization of a wideband delay line (a) and a dual-resonator sensor (b), both compatible with differential measurement approaches.

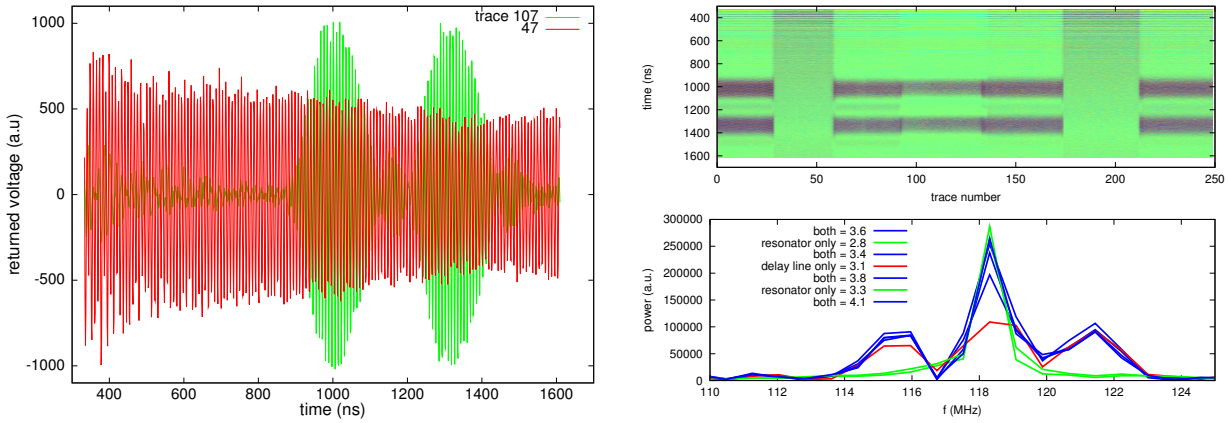

(a) (b)

FIG. 2. Experimental measurement of the response of a delay line ((a), green) and a 100 MHz fundamental frequency resonator ((a), red) as probed by a Malå RAMAC GPR unit. (b) A radargram is made of multiple A-scan RADAR traces (fast time vertical, trace number horizontally). The sequence of experiments is with the delay line and resonator (both), resonator only, delay line and resonator, delay line only, and again delay line and resonator (both), resonator only, delay line and resonator. Bottom (b): Fourier transform of the recovered signal in the various configurations just described: the peaks of equal areas whatever the sensor configuration emphasizes that both resonators and delay line exhibit similar efficiency to returning energy when excited by the wideband incoming RADAR pulse. The value next to each legend entry is the integral below each curve, representative of the returned power (arbitrary units).

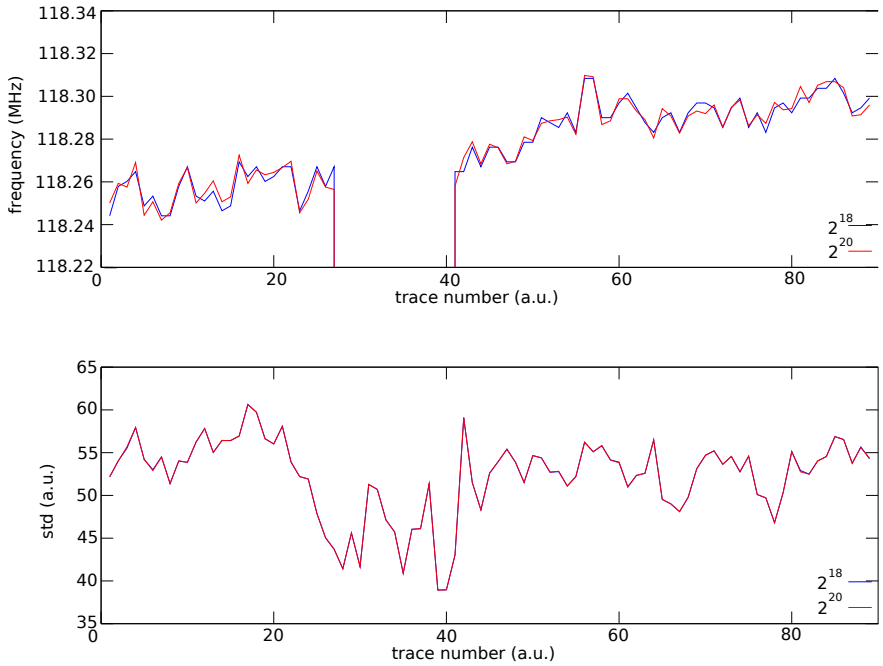

FIG. 3. Result of applying the LASSO estimator algorithm using the sparse sine wave distribution in the spectrum. Top: the frequency estimate as a funtion of trace number. Each estimate is independently computed and the standard deviation is 7.8 kHz, with a result independent of the dimension $\mathcal{K}$ for values larger than 2^{18} (here shown for 2^{18} and 2^{20}). The frequency resolution is thus 100-fold improvement with respect to the Fourier transform (613 MHz sampling rate, 800 sampled points). Notice that the frequency estimate loss between traces 25 and 41 is consistent with the removal of the resonator from the GPR interrogation range. Bottom: estimate of the standard deviation of the additive noise σ_ϵ.

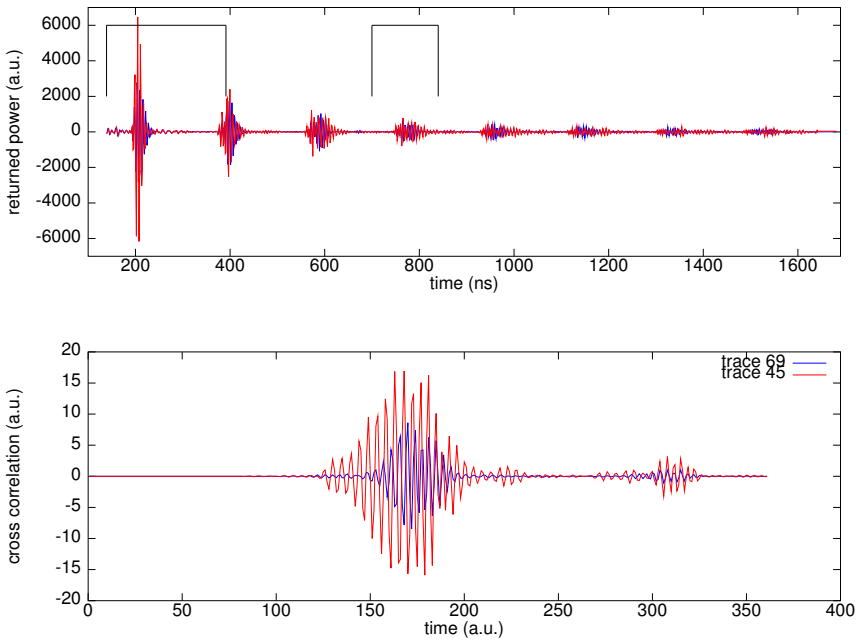

FIG. 4. Top: raw measurements recorded by a GPR operating at 200 MHz, with a HBAR sensor located at a fixed distance between the emitting and receiving antennas (bistatic configuration, the antennas being separated by 50 cm). Bottom: results of the cross-correlation computation between the segments indicated by horizontal lines on the top graph (first and fourth reflections, selected for maximum separation and thus maximum delay while keeping acceptable signal to noise ratio). The cross-correlation maximum, locally fitted by a parabolic fit for sub-pixel resolution, provides an accurate estimate of the time delay between the two returned pulses, and thus the physical quantity changing the acoustic velocity. Notice the cross correlation maximum position varying as a function of the HBAR temperature.

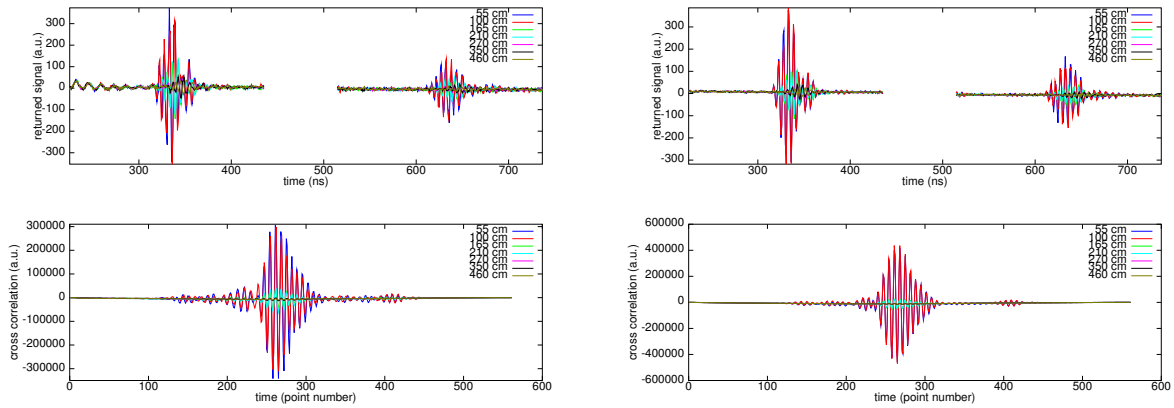

(a) (b)

FIG. 5. Interrogation of a HBAR sensor buried at varying distances from the surface in a snow drift assumed to remain at constant temperature during the measurement. The HBAR response is considered in the time domain as multiple reflections of the incoming GPR pulse. Top: time domain returned signals. Bottom: the cross correlation of two returned signal echos performs a matched filter identification providing both efficient signal extraction from noise and accurate delay identification through the position of the cross-correlation. Using both 100 and 200 antennas *on the same transducer* acting as remote cooperative target, the device was still visible while buried as deep as 5 m below the surface at which the GPR antennas were located. (a) Measurements of the HBAR using a 100 MHz antenna. (b) Measurements of the *same* device using a 200 MHz antenna. Notice the cross correlation maximum value decay with distance, but most significantly the cross-correlation maximum position varying as a function of the target distance to the GPR antennas. The distance value next to each legend entry is the depth of the sensor with respect to the antennas located on the snow drift surface, ranging from 55 cm to 460 cm.

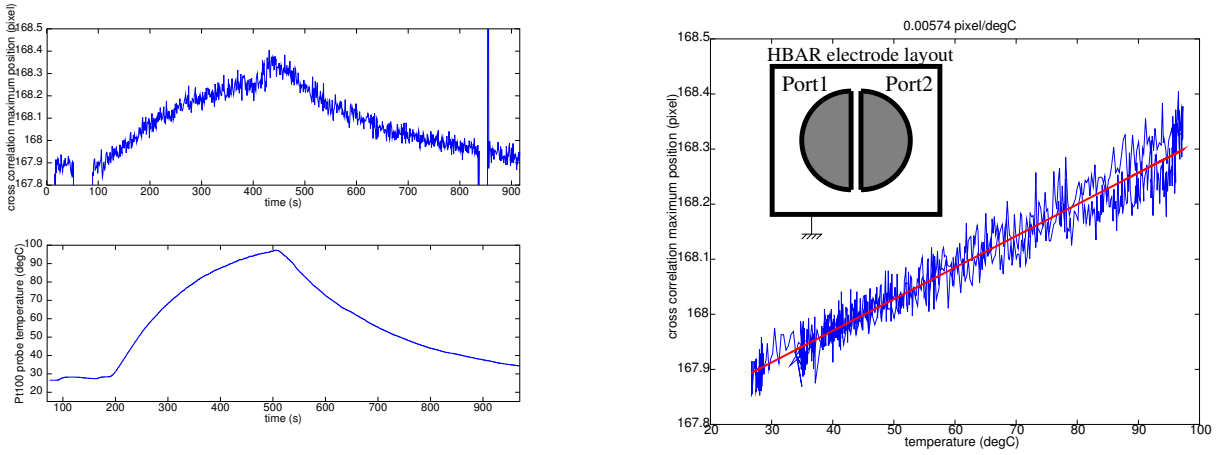

(a) (b)

FIG. 6. (a) Top, GPR based interrogation of a HBAR sensor subject to temperature variations using a resistance as a heater and located at a fixed distance from the antennas. Bottom: the temperature of the acoustic sensor was simultaneously measured using a Pt100 reference probe. In this example, the distance between HBAR and RADAR is kept constant and the temperature is varied. (b) Time delay *v.s.* temperature between two pulses relationship as observed on this particular device. Considering the slope of the temperature v.s delay dependence (left) is 5.7×10^{-3} K^{-1} and the delay standard deviation (right), the temperature measurement standard deviation is 4.6 K, with 8 stack averaging on the GPR trace acquisition and no sliding average on the temperature estimated values. Inset: electrode layout for a coupled resonator configuration, with a typical chip size of 1×1 mm^2 and electrode diameter of 900 μm.

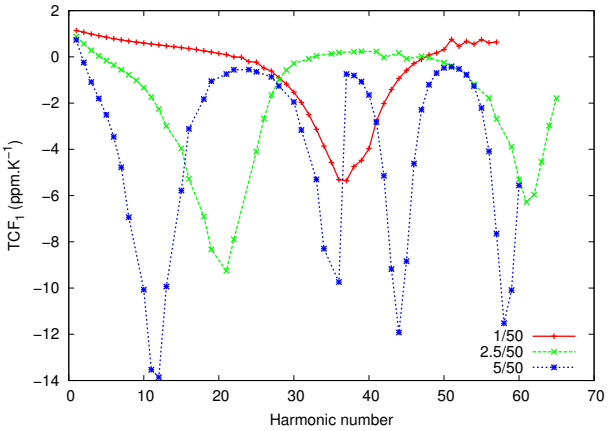

FIG. 7. Simulation of the evolution of the first order temperature coefficient of an HBAR made of a (YXl)/165^o lithium niobate thin single-crystal piezoelectric layer over a 50 μm thick (YXl)/35^o quartz as a function of overtone number. The thinner the piezoelectric active layer, the lower the temperature coefficient variation as a function of overtone number, providing easier data processing when using the sensor with various GPR antennas (the same temperature coefficient is used whatever the operating frequency), but preventing a differential approach in a restricted frequency range for which different temperature sensitivities of the various echos is needed.

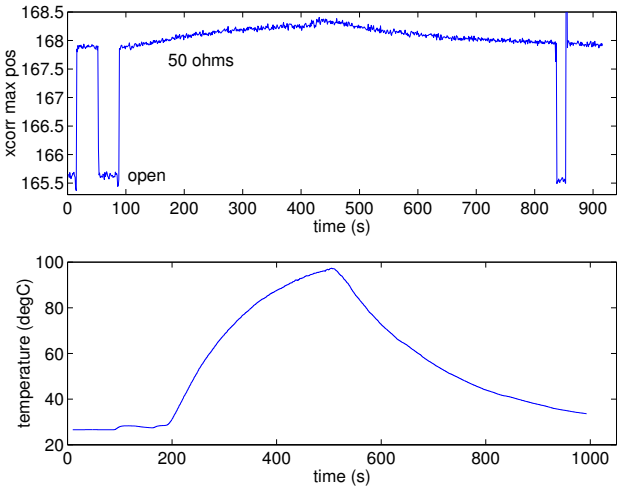

FIG. 8. The device used earlier (Fig. 6) as a dipole was used as a 4-pole coupled oscillator. The second port was either loaded by a 50 Ω load, or opened. The switch behavior probed through a wireless link is dominant over the temperature variation in the 20-80 ^{o}C range.

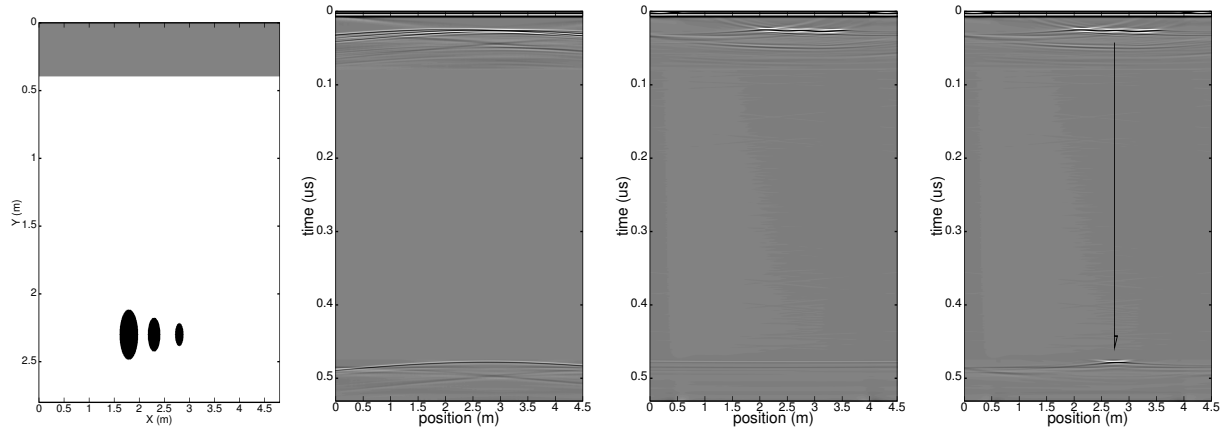

(a) (b) (c) (d)

FIG. 9. (a) geometrical model considered, with 3 perfectly conducting cylinders (black) 1.9 m deep and separated by 50 cm, in dry sand ($\varepsilon_r = 3$, white), the middle rebar being fitted with an acoustic transducer delaying its echo by 450 ns (air above the surface is indicated as a grey area). (b) raw modelled response, (c) Stolt migration of the previous graph assuming a velocity of 163 m/μs. While the hyperbolas from the reflection on the rebars converge towards a blured set of reflections from the three conducting cylinders (time before 80 ns), the hyperbola located near 500 ns delay does not converge since its curvature does not fit the expected shape from an electromagnetic delay at such a large distance. (d) separate migration of the three reflections from the rebars as in the middle graph, and in addition the delayed echo is manually migrated by shifting the time origin by 450 ns. In this case, the hyperbola translated by 450 ns converges to a single reflector well identified with the middle rebar, at abscissa 2.70 m (arrow). This basic simulation only assumes that the direct wave reaching the sensor generates an acoustic signal which is returned to the GPR receiver without additional reflections on other buried dielectric interfaces.

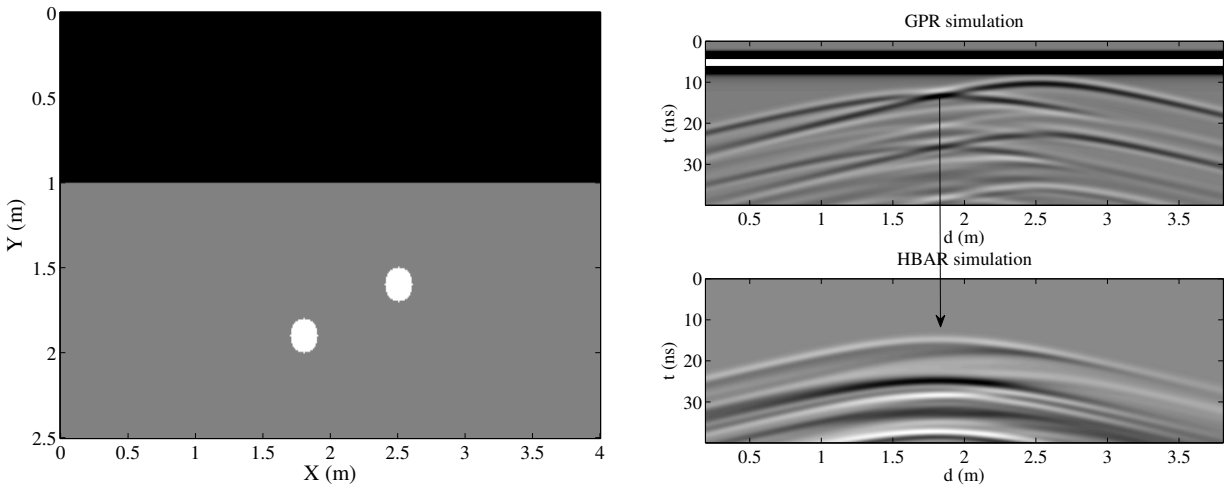

(a) (b)

FIG. 10. (a) Geometry of the modelled configuration, in which two water ($\varepsilon_r = 81$) filled pipes (white) are buried 0.9 and 0.6 m deep in dry sand (grey, $\varepsilon_r = 2.25$). The acoustic transducer is assumed to be located atop the deepest pipe. (b) Top: RADARgram obtained by scanning the transmitter and the receiver over the surface, at the air (black)-sand (grey) interface. The hyperbola generated by the shallowest tube nearly overlaps the hyperbola generated by the deepest tube, making the identification process of the buried structure complex. Bottom: the signal recorded by the acoustic transducer located on top of the deepest tube records the incoming signal, and re-emits the recorded sequence after some delay representative of the acoustic wave propagation in the transducer. The hyperbola related to the deepest tube in now well resolved (vertical arrow). Since the electromagnetic signal propagation from the surface to the sensor step and the propagation from the sensor to the surface step are separate, the direct air-wave from emitter to receiver is no longer visible on the bottom graph.